Bonding character, electron delocalization, and aromaticity of cyclo[18]carbon (C_{18}) precursors, C_{18}-$(CO)_n$ (n = 6, 4, and 2): Focusing on the effect of -CO groups

Xia Wang [a], Zeyu Liu [a,*], Xiufen Yan [a], Tian Lu [b,*], Weiwei Xiong [a,*]

[a]*School of Environmental and Chemical Engineering, Jiangsu University of Science and Technology, Zhenjiang 212100, People's Republic of China*

[b]*Beijing Kein Research Center for Natural Sciences, Beijing 100022, People's Republic of China*

[*]Corresponding author. E-mail: liuzy@just.edu.cn (Zeyu Liu); sobereva@sina.com (Tian Lu); xiongweiwei@just.edu.cn (Weiwei Xiong)

Abstract

Although the unique cyclo[18]carbon (C_{18}) realized by recent experiments has been greatly concerned, it has so far remained elusive. In contrast, its precursors C_{18}-$(CO)_n$ (n = 6, 4, and 2), which can be separated stably, are of more practical significance. In this paper, the bonding character, electron delocalization, and aromaticity of the C_{18}-$(CO)_n$ (n = 6, 4, and 2) with out-of-plane and in-plane dual π systems (π^{out} and π^{in}) perpendicular to each other are studied by combining quantum chemical calculations and wavefunction analyses. These cyclocarbon oxides exhibit alternating long and short C-C bonds and extensive electron delocalization, and a significant diatropic induced ring current under the action of external magnetic field is therefore observed, which reveals the aromatic characteristic in the molecules. The global electron delocalization and significant influence of the number of intramolecular carbonyl (-CO) on the two sets of π conjugated systems have been focused on, and the essential reason for the distinct difference in the overall aromaticity of the molecules was also clarified. It seems that the substituent -CO groups hinders the electron delocalization of the π^{in} system but has relatively small effect on the π^{out} system, resulting in the molecules with less -CO group showing greater aromaticity.

Table of contents (TOC) graphic:

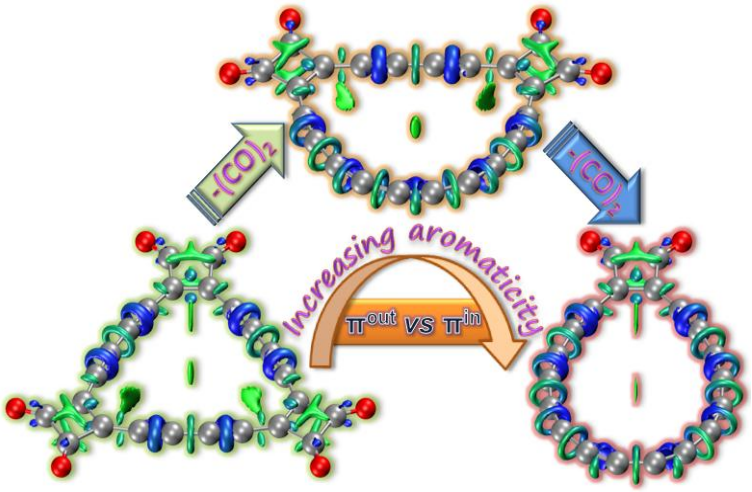

Keywords: cyclo[18]carbon precursors, electronic structure, bonding character, electron delocalization, aromaticity

1. Introduction

Cyclo[18]carbon (C_{18}) is a novel all-carboatomic molecule that has been generated and characterized recently [1,2]. This allotrope of carbon has attracted considerable attention in the field of chemistry and material science since it has been observed in condensed phase [3-39], and a large number of theoretical explorations on its electronic structure [3-5], aromaticity [4,6-12], optical and spectroscopic properties [5,13-15], molecular interaction [16,17], potential applications in molecular devices [8,18-21], as well as multiple properties of its analogues [7-9,11,14,15,22] have been reported in succession. However, there is currently no way to obtain an isolate product of C_{18} and its pure-carbon analogues due to their extreme chemical activity.

In fact, since Hoffmann put forward the idea of C_{18} in 1966 [40], several strategies have been proposed to try to achieve this unique allotropic carbon, including synthesis by eliminating the heteroatomic substituents of its various cyclocarbon precursors through methods such as retro-Diels-Alder reaction [41], decomplexation [42], decarbonylation [43], and [2+2] cycloreversion [44]. One of the two recent pioneering experiments to prepare C_{18} was achieved by sequentially removing a pair of carbonyl groups [$(-CO)_2$] from a cyclocarbon oxide C_{18}-$(CO)_6$, producing the C_{18}-$(CO)_4$ and C_{18}-$(CO)_2$ molecules in turn, up to the final product C_{18} [1]. Actually as early as 30 years ago, Diederich and co-workers have successfully prepared C_{18}-$(CO)_6$ molecule and determined it by X-ray diffraction with the same purpose [43]. However, although cyclocarbon oxides are very special compounds with rich-carbon features, maybe blinded by the pursuit of pure all-carboatomic rings, they have not received the attention they deserve. And yet we believe that, at least till now, studying the easily synthesized and relatively stable cyclocarbon oxides C_{18}-$(CO)_n$ (n = 6, 4, and 2) should have more practical significance than investigating the very reactive and hardly attainable C_{18}.

Our previous theoretical studies on all-carboatomic C_{18} showed that, due to the special *sp*-hybrid form of its carbon atoms, the molecule exhibits an unusual in-plane π electron system (π^{in}) in addition to the out-of-plane π system (π^{out}) that are common

in conjugated molecules [5,10,15]. It can be expected that the cyclocarbon oxides should possess the special electronic structure that interests us like C_{18}. In addition, it is a meaningful topic to explore how the presence of -CO groups affects the electron delocalization and aromaticity of the cyclocarbon oxides. So, in this work, the bonding character and electron delocalization of three C_{18} precursors, C_{18}-$(CO)_n$ (n = 6, 4, and 2), are analyzed in detail using a variety of wavefunction analysis methods based on reliable quantum chemistry calculations. Their respective aromatic characteristics will be discussed and compared in terms of the number of -CO groups. The in-depth study of the properties of C_{18}-$(CO)_n$ (n = 6, 4, and 2) molecules may be beneficial to deepen the understanding of the systems and thereby facilitate making them applied in practice.

2. Computational Details

All results presented in this work were calculated at the ωB97XD [45]/def2-TZVP [46] level in the gas phase. Gaussian 16 (A.03) program was employed for the density functional theory (DFT) calculations [47].

The anisotropy of the current-induced density (ACID) analysis [48] was realized by the ACID code based on the output file of Gaussian program, and the maps were generated by POV-Ray render [49]. The gauge-including magnetically induced currents (GIMIC) analysis [50] was finished via the GIMIC code based on the formatted check point file of Gaussian program, and the maps and animations were rendered by ParaView visualization program [51]. Other electronic structure and wavefunction analyses were performed with the Multiwfn 3.8(dev) code [52] based on the wavefunctions produced by DFT calculations. The isosurface maps of various orbitals and real space functions were rendered by means of Visual Molecular Dynamics (VMD) software [53] based on the cube files exported from Multiwfn. The colored contour maps of various real space functions were plotted directly via the Multiwfn code.

For the convenience of visualization, the molecules in all structural and isosurface

diagrams in this paper are placed on the XY-plane and presented at a 45 º angle relative to the paper surface.

3. Results and Discussion

3.1. Calibration of computational strategy

Previous theoretical studies on the molecular structure of C_{18} have demonstrated that only the exchange-correlation functionals with more than 25% Hartree-Fock exchange can reliably exhibit the ground-state geometry of the molecule [4,10], and the ωB97XD/def2-TZVP level has been proved to robustly reproduce the high-precision computational result and experimental observation. Hence, we still adopt the same strategy as our previous works on C_{18} to optimize the geometry of precursors C_{18}-$(CO)_n$ (n = 6, 4, and 2).

The geometric structures of the precursors C_{18}-$(CO)_n$ (n = 6, 4, and 2) obtained at the ωB97XD/def2-TZVP level are shown in Fig. 1, and the corresponding Cartesian coordinates are listed in Table S1. The optimized structures of all precursor molecules are found to be strictly planar with no imaginary frequencies, and the point group symmetries of C_{18}-$(CO)_n$ with n = 6, 4, and 2 are D_{3h}, C_{2v}, and C_{2v}, respectively. Fig. S1 summarizes the calculated structural parameters and available crystal data of C_{18}-$(CO)_6$ molecule. The maximum absolute deviations of bond lengths and bond angles between theoretical calculation and experimental measurement are only 0.03 Å and -2.3 º, respectively, which shows that our calculations accurately reproduced the crystal structure of the C_{18}-$(CO)_6$. This also emphasizes that the exchange-correlation functional of ωB97XD is a reliable choice for the studying of C_{18} and its substitutes.

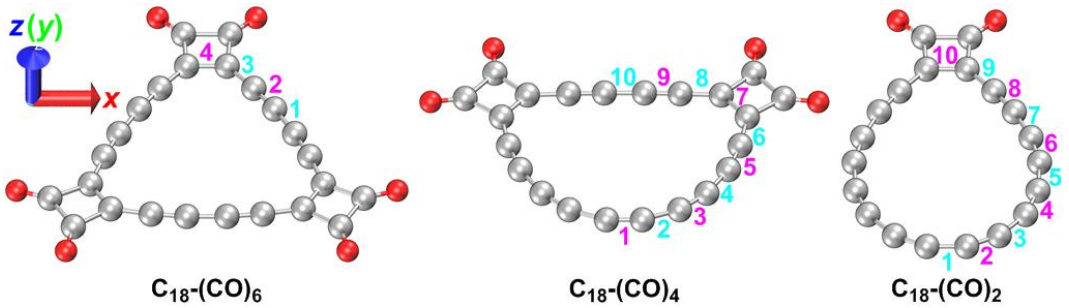

Fig. 1 Geometric structure of C_{18}-$(CO)_n$ (n = 6, 4, and 2) studied in the present work. C atoms are in gray and O atoms are in red. Also shown are the Cartesian axis and bond indices. Long bond indices are in cyan and short bond indices are in pink.

3.2. Character of electronic structure

From a structural point of view, the C_{18}-$(CO)_n$ (n = 6, 4, and 2), like C_{18} ring, present a polyynic skeleton with alternating long and short bonds. Based on the geometry and wavefunction generated at the level of ωB97XD/def2-TZVP, we simulated the scanning tunneling microscope (STM) image of the precursors C_{18}-$(CO)_n$ (n = 6, 4, and 2) in the gas phase, as displayed in Fig. S2. It can be seen that the tunneling current is relatively prominent over the short C-C bonds, corresponding to gray or white on the STM image. In contrast, almost no tunneling current is detected on the long C-C bonds, because the local density-of-state (LDOS) of the highest occupied molecular orbitals (HOMOs) show nodal planes in these regions. This character of STM of cyclocarbon oxides is very similar to that of C_{18}, exhibiting similarity between their electronic structures [10]. For details and meanings of STM image simulation, please refer to the supplementary material of Ref. [10].

Bond order is an important concept and a quantitative index for characterizing chemical bonds, which essentially reflects the number of electron pairs shared by two bonding atoms. Here, we calculated various bond orders of C_{18}-$(CO)_n$ (n = 6, 4, and 2) via different methods, and the bond lengths and bond orders of each precursor are collectively plotted in Figs. S3-S5. It is found that there is a good correlation between bond length and various bond orders of each species, that is, the longer the C-C bond length is, the smaller the C-C bond order is, and vice versa. Similarly to the case of

C_{18}, the bond orders of the long and short bonds in C_{18}-$(CO)_n$ (n = 6, 4, and 2) calculated by all methods are larger than 1.0 and smaller than 3.0, respectively, suggesting that some of the electrons from the short C-C bonds, which are formally triplet bond, are delocalized to the long C-C bonds. The existence of electron delocalization in C_{18}-$(CO)_n$ (n = 6, 4, and 2) implies that it is possible for them to generate induced ring current in external magnetic field, which is the topic we will focus on below.

In addition to the commonly known π^{out} molecular orbitals (MOs), molecules containing successive *sp*-hybrid carbons usually have a special conjugated π^{in} orbitals located in the molecular plane [5,10,15]. The π^{out} and π^{in} MOs of C_{18}-$(CO)_n$ (n = 6, 4, and 2) molecules are listed in Figs. S6-S8, which will be involved in the following wavefunction analysis.

The interaction region indicator (IRI) is a simple real space function that can clearly reveal both chemical bonds and weak interactions between atoms or molecular fragments [54]. The isosurfaces and color-filled maps of IRI function for the π MOs, referred to as IRI-π, are depicted in Fig. 2. It can be seen that the IRI-π isosurface of the C-C bonds in the ring except for those adjacent to the -CO groups is annular, indicating that these C-C bonds have dual π (i.e. π^{out} and π^{in}) interaction features. However, the strength of π interaction of two types of C-C bonds is obviously different. The annular IRI-π isosurface of the short C-C bonds is broader and bluer than that of the long C-C bonds, providing intuitive evidence for the larger electron density in the π interaction region of the short ones, so the π interaction of the short bonds is stronger. In contrast, since the corresponding IRI-π isosurface is obviously not annular, only π^{out} interactions exist on the C-C bonds adjacent to the -CO groups. Given all this, it can be inferred that only π^{out} electrons should be responsible to the overall electron delocalization over the whole molecular skeleton. The color-filled maps can give the same conclusion as isosurface graphs from another perspective.

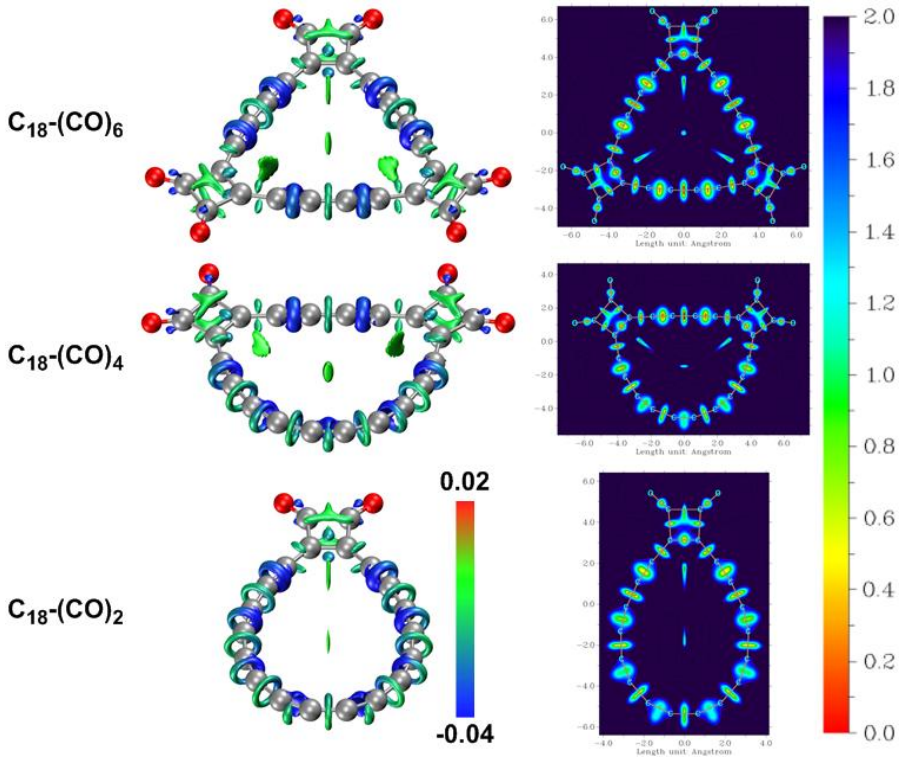

Fig. 2 Isosurfaces (isovalue = 1.2 au) and color-filled maps at 0.5 Å above the ring of IRI-π of C_{18}-$(CO)_n$ (n = 6, 4, and 2). The scales of color bars are in au.

3.3. Orbital interaction analysis

The MOs of C_{18}-$(CO)_n$ can be considered as the result of mixing the MOs of the -CO and C_{18}- fragments. The analysis of the interaction between the fragment MOs in C_{18}-$(CO)_n$ is helpful to deeply understand the interruption of π^{in} electron delocalization at carbon ring near the -CO groups. The orbital interaction diagram in Fig. 3 clearly exhibits how crucial frontier MOs of C_{18}-$(CO)_2$ are constructed from fragment MOs.

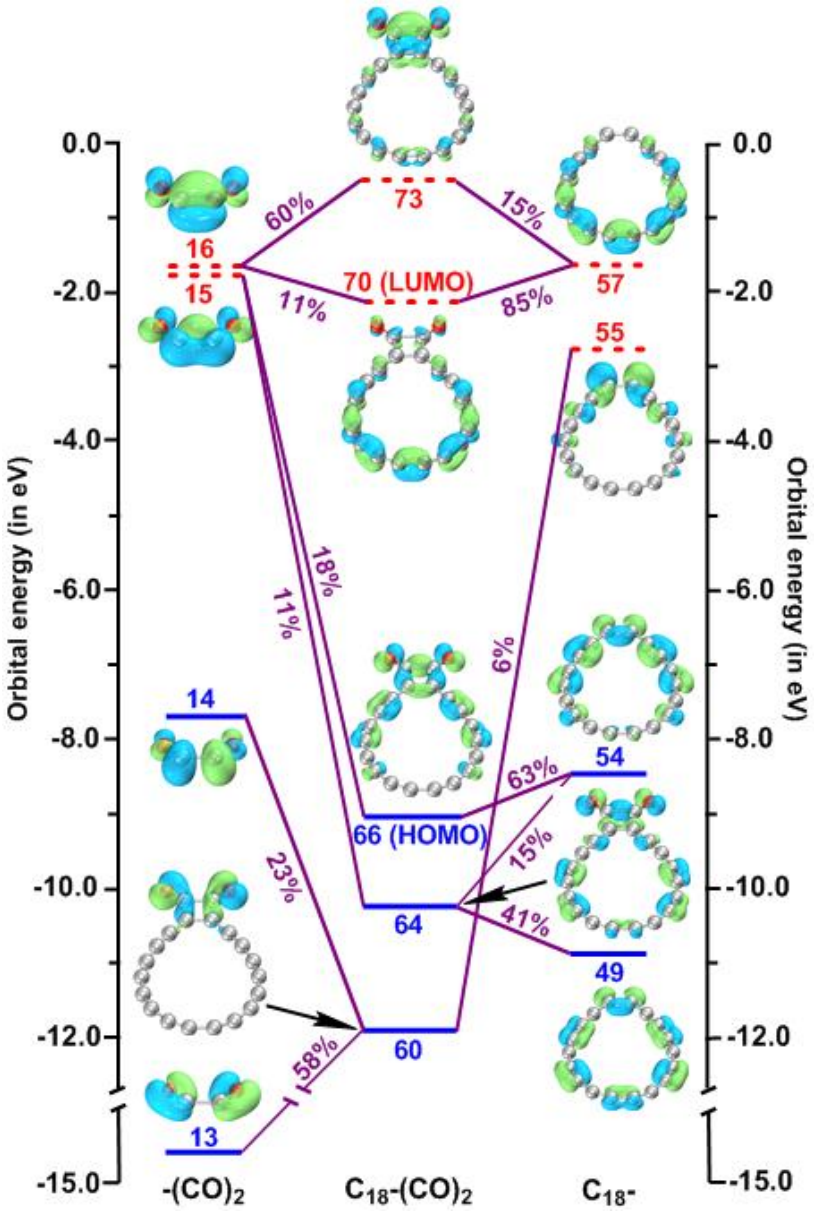

Fig. 3 Orbital interaction diagram of C_{18}-$(CO)_2$. Blue solid and red dashed bars correspond to occupied and virtual MOs, respectively. The MOs are plotted as isosurface graphs with isovalue of 0.05. Blue texts mark orbital indices. Purple texts indicate major contribution of MOs from the fragments to the C_{18}-$(CO)_2$.

As shown in the previous IRI-π analysis and the subsequent electron delocalization analyses, after the combination of $(CO)_2$ and C_{18} , the π^{in} electron conjugation is destroyed around the junction region between the two fragments. Two underlying reasons are: (1) the introduction of the -CO groups causes obvious

distortion on the C_{18} structure, especially makes severe in-plane bending of the C-C-C angles in the carbon ring near the -CO groups, which leads to evident difficulty in π^{in} electron conjugation over this region; (2) as can be seen in Fig. 3, the MOs of -$(CO)_2$ and the π^{in} orbitals of C_{18}- produce a significant mixing, resulting in new occupied MOs of C_{18}-$(CO)_2$ clearly display the character of σ bonds between the -$(CO)_2$ and C_{18}- moieties. Since σ electrons are well known to be strongly localized, the originally globally delocalized π^{in} electrons in C_{18} can no longer delocalize over the bonds where carbon ring binds to the two -CO groups.

3.4. Character of electron delocalization

The localized orbital locator (LOL) [55] and electron localization function (ELF) [56] proposed by Becke et al. are quite popular real space functions for determining the characteristics of electron localization/delocalization in chemical systems.

The isosurfaces of LOL for the occupied π^{out} and π^{in} MOs, respectively referred to as LOL-π^{out} and LOL-π^{in}, are displayed in Fig. 4. The isosurfaces of LOL-π^{out} clearly show the favorable global delocalization channels of the electrons in π^{out} MOs, and those around short C-C bonds are much broader than around long C-C bonds, indicating that the electron delocalization over the short C-C bonds is more prominent. As the number of -CO groups in precursors decreases from n = 6 to 4 and then 2, the value of bifurcation of the LOL-π^{out} isosurfaces gradually increases, which means that the π^{out} electron delocalization of the molecule enhances sequentially. However, the isosurfaces of LOL-π^{in} are truncated near the -CO groups, and the hindrance to the electron delocalization of the molecule with more -CO substituents is more severe. Therefore, π^{in} MOs in C_{18}-$(CO)_n$ (n = 6, 4, and 2) only exhibit a local rather than global delocalization, and C_{18}-$(CO)_2$ shows a relatively more complete delocalization than its analogues. Similarly to that of π^{out} systems, the electron delocalization of π^{in} MOs on the short C-C bonds is also more pronounced than that on the long bonds. By comprehensively considering the electron delocalization characteristics of π^{out} and π^{in} MOs, we can infer that the overall electron delocalization of C_{18}-$(CO)_n$ (n = 6, 4, and

2) molecules must be weaker than that of C_{18} ring with extensively global delocalization of both set of π orbitals, and the order of electron delocalization extent for C_{18}-$(CO)_n$ (n = 6, 4, and 2) is: C_{18}-$(CO)_6$ < C_{18}-$(CO)_4$ < C_{18}-$(CO)_2$.

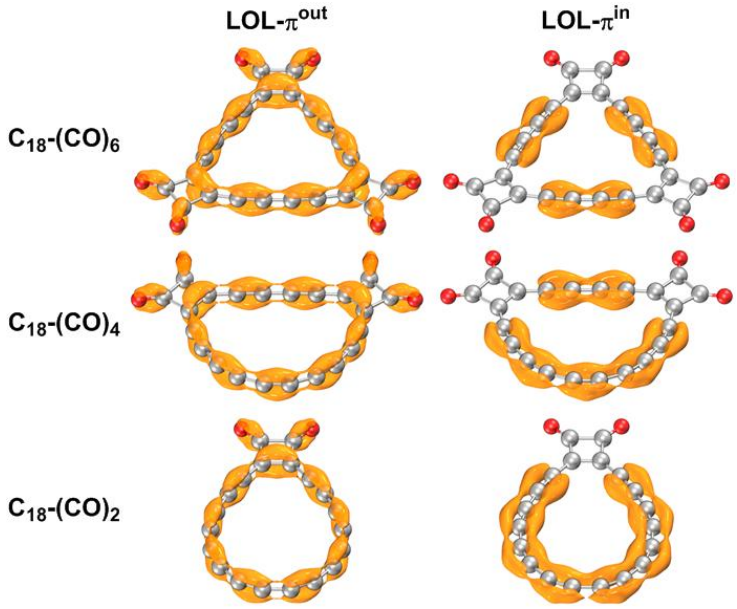

Fig. 4 Isosurfaces of LOL-π of C_{18}-$(CO)_n$ (n = 6, 4, and 2). The isovalues are set to be their respective bifurcation value (see Table S2) of isosurface except for the breakpoint near -CO groups.

The color-filled maps of LOL-π^{out} at 0.5 Å above the ring as well as LOL-π^{in} on the ring plane of C_{18}-$(CO)_n$ (n = 6, 4, and 2) molecules are plotted in Fig. 5 for presenting the π-electron delocalization from another perspective. These contour maps show, more clearly, the difference in electron delocalization around long and short C-C bonds in the carbon ring of different molecules as well as the truncation feature of LOL-π^{in} near the -CO groups, which are consistent with the above conclusions drawn based on isosurface maps.

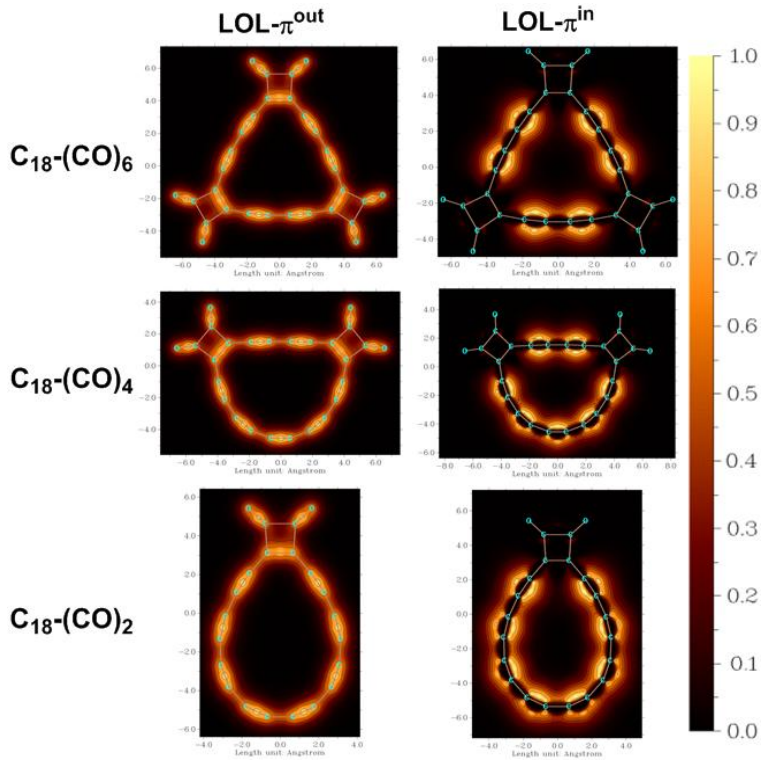

Fig. 5 Color-filled map (in au) of LOL-π^{out} at 0.5 Å above the ring and LOL-π^{in} on the ring plane of the C_{18}-$(CO)_n$ (n = 6, 4, and 2). The scales of color bars are in au.

The isosurfaces and color-filled maps corresponding to the ELF function for π MOs (referred to as ELF-π^{out} and ELF-π^{in}) are shown in Figs. S9 and S10. The electron delocalization characteristics described by the ELF-π function are fairly similar to those by LOL-π, although the definition of ELF has a different physical idea from LOL, which further confirms our previous inference about the characteristics of electron delocalization.

3.5. Response to external magnetic field and molecular aromaticity

Generally, a closed circle molecule with electron delocalization over it will produce a unidirectional ring current under the induction of an external magnetic field, and the strength of the induced current reflects the strength of its aromaticity. Next, we will discuss and compare the aromaticity of C_{18}-$(CO)_n$ (n = 6, 4, and 2) by analyzing their response to external magnetic field.

Anisotropy of current-induced density (ACID): The anisotropy of

current-induced density (ACID) is an intuitive and universally applicable method for visual analysis of electron delocalization by generating molecular ring current induced under a given external magnetic field [48], which can be further decomposed into the contributions of different types of molecular orbitals to gain a deeper insight. The ACID isosurfaces of π^{out} and π^{in} electrons, respectively referred to as ACID-π^{out} and ACID-π^{in}, in C_{18}-$(CO)_n$ (n = 6, 4, and 2) are plotted in Fig. 6.

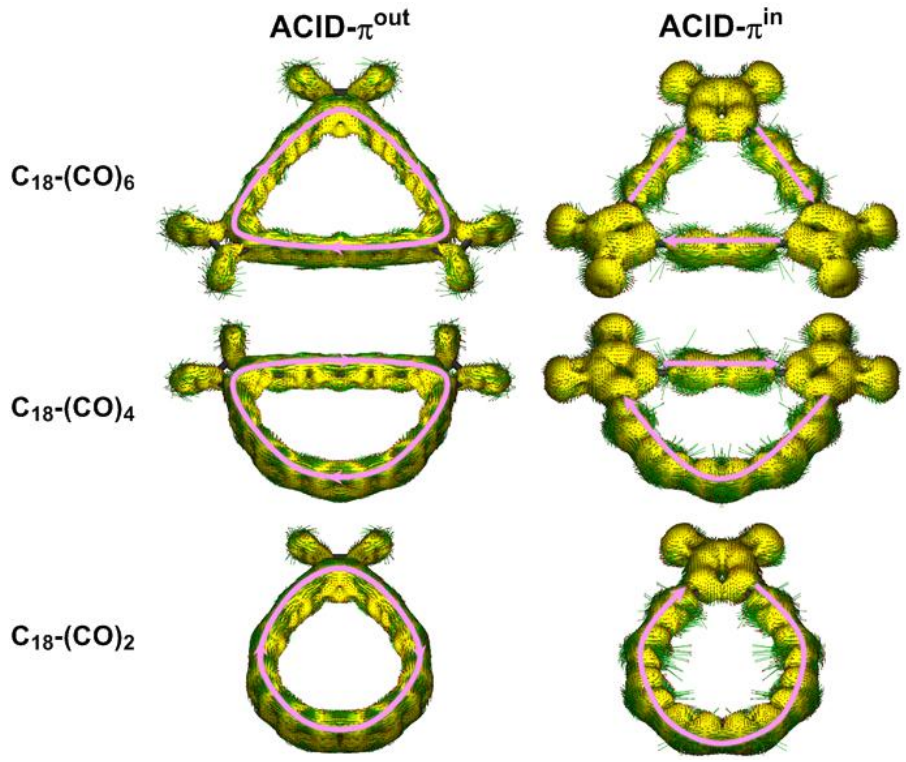

Fig. 6 Isosurfaces (isovalue = 0.03 au) of ACID of C_{18}-$(CO)_n$ (n = 6, 4, and 2). The external magnetic field is perpendicular to the ring plane and points outward. The green arrows represent direction and magnitude of the induced current at various positions on the ACID isosurfaces.

It can be seen that the π^{out} electrons of all three precursors show complete and obvious diatropic ring currents, which conform to the left-hand rule with the direction of the external magnetic field. The unidirectional ring currents caused by π^{out} electrons are basically distributed at the region above/below the ring. This observation provides strong evidence for the out-of-plane aromaticity of the C_{18}-$(CO)_n$ (n = 6, 4, and 2). Furthermore, the ACID-π^{out} isosurface of the precursors widens and the ring current density increases with the decrease of number of -CO groups in the molecule,

indicating that the molecular aromaticity created by π^{out} electrons gradually strengthens in the order of C_{18}-$(CO)_6$ < C_{18}-$(CO)_4$ < C_{18}-$(CO)_2$. The ACID isosurface of the π^{in} electron system, namely ACID-π^{in}, in the molecules shows the truncation of the in-plane ring current near the -CO groups. In particular, the increase of the number of -CO groups results in an enhanced hindrance of global ring current and leads to more appearance of multidirectional local induced currents.

The ACID diagrams that take into account all π (i.e., π^{out} and π^{in}) electrons in the system are shown in Fig. S11, from which it can be seen that the induced current intensity of these precursors is consistent with the extent of electron delocalization obtained from the previous analysis, namely C_{18}-$(CO)_6$ < C_{18}-$(CO)_4$ < C_{18}-$(CO)_2$.

Gauge-including magnetically induced current (GIMIC): The gauge-including magnetically induced current (GIMIC) is another effective method to reveal the induced current of chemical systems under action of external magnetic field [50]. The GIMIC maps on the ring plane of C_{18}-$(CO)_n$ (n = 6, 4, and 2), which provides a complementary perspective on aromaticity from the ACID isosurface, are displayed in Fig. 7. It is clear that the significant diatropic/paratropic currents formed inside/outside the ring for each precursor, from which we can draw the same conclusion as that from ACID analysis that the precursor molecules are all considered to be aromatic.

Based on the vector field of ring current generated by the GIMIC code, the induced ring current of a system can be vividly shown in the form of animation, which enables one to observe the dynamic characteristics of the induced ring current very intuitively. We have provided the animation files of induced current for the three precursors in supplementary material, which are strongly recommended to the readers for viewing.

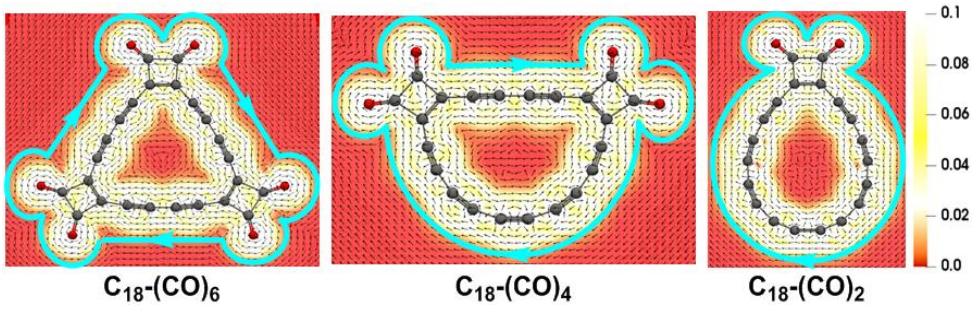

Fig. 7 GIMIC map on the ring plane of C_{18}-$(CO)_n$ (n = 6, 4, and 2). The external magnetic field is perpendicular to the ring plane and points outward. The black arrows and background colors respectively indicate the direction and magnitude of induced current at various positions. The color scale is given in au.

Iso-chemical shielding surface (ICSS): The iso-chemical shielding surface (ICSS) [57] is a real space function extending the idea of the well-known nucleus-independent chemical shifts (NICS) [58] to three-dimension case, which can clearly reveal the extent of magnetic shielding/deshielding in different regions caused by delocalized π electrons.

The isosurface and color-filled map of the ZZ component of ICSS, referred to as $ICSS_{ZZ}$, for the three precursors C_{18}-$(CO)_n$ (n = 6, 4, and 2) are shown in Fig. 8. It can be seen that there is a shielding area inside the ring protruding in the direction perpendicular to the ring plane, surrounding by a toroidal deshielding area outside the ring. The shielding/deshielding characteristics of C_{18}-$(CO)_n$ (n = 6, 4, and 2) once again indicate that they should be considered as a system with remarkable aromaticity, since typical aromatic systems share the same feature of $ICSS_{ZZ}$ [10]. From the figure it is obvious that the peripheral deshielding region of each molecule is interrupted by the -CO groups, and the more -CO groups there are, the more severe the interruption is. The reason for this is clearly explained by the previous orbital interaction analysis, that is the existence of the -CO groups breaks the conjugation of π^{in} electrons and hence the corresponding in-plane induced current. The strong interference of magnetic shielding characteristics is therefore generated. Note that from color-filled map in Fig. 8, the color inside/outside the ring become redder/bluer with decrease of the number of -CO groups, displaying stronger shielding/deshielding effect. This observation clearly demonstrates that from C_{18}-$(CO)_6$ to C_{18}-$(CO)_4$ then C_{18}-$(CO)_2$, the molecule becomes more and more aromatic.

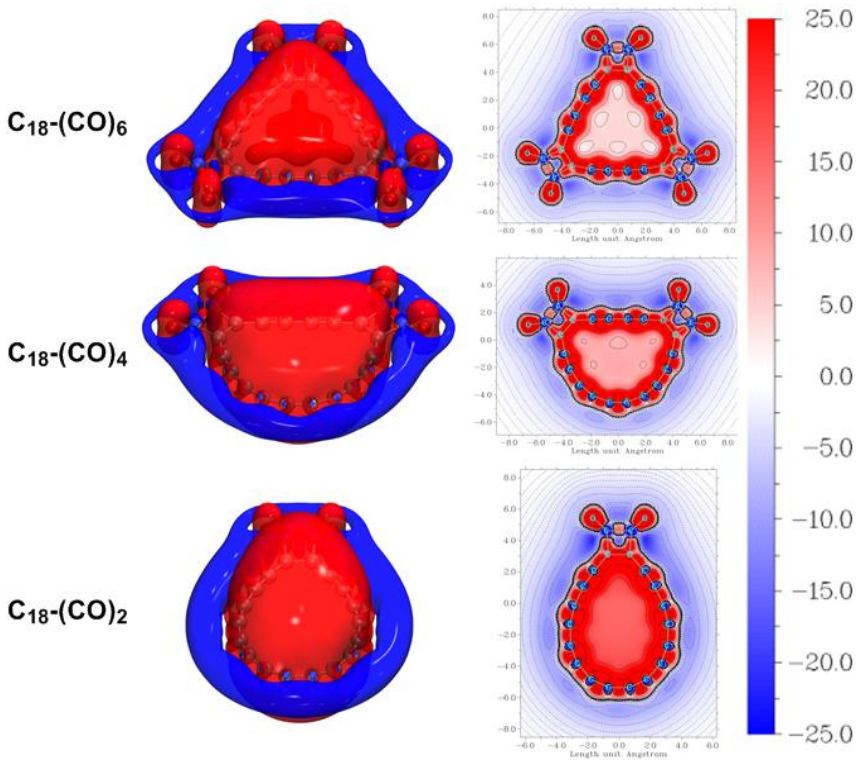

Fig. 8 Isosurfaces (isovalue = 8.0 ppm) and color-filled maps on molecular plane of $ICSS_{ZZ}$ of C_{18}-$(CO)_n$ (n = 6, 4, and 2). The color scale is given in ppm.

The $ICSS_{ZZ}$ values calculated at 1 Å above the center of the ring, referred to as $ICSS_{ZZ}(1)$, is quite robust and popular for quantitatively determining aromaticity of ring systems. The $ICSS_{ZZ}(1)$ values of C_{18}-$(CO)_n$ (n = 6, 4, and 2) are observed to be 4.0, 7.8, and 15.3 ppm for n = 6, 4, and 2, respectively, which are lower than that of C_{18} (23.7 ppm) and benzene (29.9 ppm) [10], indicating that a relative weak but still distinct aromaticity in the molecules. The order of aromaticity strength determined by the $ICSS_{ZZ}(1)$ is also fully consistent with the judgment results from all above visual analyses.

4. Conclusions

The bonding character, electron delocalization, and aromaticity of C_{18} precursors, C_{18}-$(CO)_n$ (n = 6, 4, and 2), are theoretically explored in depth by using DFT calculations and a variety of wavefunction analyses methods. The optimized geometry

and various bond orders indicate that the cyclocarbon skeleton of the precursors shows an alternating structure of long and short C-C bonds, which is akin to C_{18}. The results of MO analysis and IRI analysis show that these molecules have two sets of π-conjugated electron systems, respectively described by π^{out} and π^{in} MOs, which provide different contributions to molecular aromaticity. The orbital interaction analysis reveals the essential reason why the introduction of -CO groups destroys the π^{in} conjugated system. Based on the analysis of LOL-π and ELF-π functions, the characteristics of electron delocalization in π^{out} and π^{in} MOs were confirmed. The ACID, GIMIC, and $ICSS_{ZZ}$ methods graphically revealed the prominent induced ring current or magnetic shielding effect of π electrons in precursors induced by external magnetic field. All the analysis methods based on the wavefunction of quantum chemistry calculations or response to external magnetic field came to exactly the same conclusion, that is, the three precursor molecules all have π^{out} electron global delocalization and π^{in} electron local delocalization, so they can be definitely classified as aromatic species, and the aromatic strength increases with the decrease of number of -CO groups.

In our opinion, it is more practical to study the easily synthesized and relatively stable precursors C_{18}-$(CO)_n$ (n = 6, 4, and 2) than the elusive C_{18}. Related research in this work can provide theoretical references for chemists to understand the properties of cyclocarbon oxides.

Author contributions

Z. Liu and T. Lu conceived the idea, designed the project, analyzed the data, and wrote the manuscript. X. Wang performed the DFT calculations and drew the diagrams under supervision of Z. Liu and W. Xiong. X. Yan participated in the draft writing.

Acknowledgments

This work was supported by National Natural Science Foundation of China for Youths

(21701059) and Natural Science Foundation of Jiangsu Province for Youths (BK20170571).

Supporting Information Available

Optimized Cartesian coordinates, optimized structural parameters and crystal structure data, STM image simulations, plot of the bond length versus bond order, isosurface map of occupied π molecular orbitals (π^{out} and π^{in}), bifurcation values of isosurface except for the breakpoint near -CO groups, isosurfaces of ELF-π, color-filled map of ELF-π^{out} at 0.5 Å above the ring and ELF-π^{in} on the ring plane, isosurfaces of ACID for all π electrons of the C_{18}-$(CO)_n$ (n = 6, 4, and 2).

References

[1] Kaiser K, Scriven LM, Schulz F, Gawel P, Gross L, Anderson HL. An sp-hybridized molecular carbon allotrope, cyclo[18]carbon. Science 2019; 365(6459): 1299–1301.

[2] Scriven LM, Kaiser K, Schulz F, Sterling AJ, Woltering SL, Gawel P, Christensen KE, Anderson HL, Gross L. Synthesis of cyclo[18]carbon via debromination of $C_{18}Br_6$. J Am Chem Soc 2020; 142(30): 12921–12924.

[3] Pereira ZS, da Silva EZ. Spontaneous symmetry breaking in cyclo[18]carbon. J Phys Chem A 2020; 124(6): 1152−1157.

[4] Baryshnikov GV, Valiev RR, Kuklin AV, Sundholm D, Ågren H. Cyclo[18]carbon: Insight into electronic structure, aromaticity and surface coupling. J Phys Chem Lett 2019; 10(21): 6701–6705.

[5] Liu Z, Lu T, Chen Q. An sp-hybridized all-carboatomic ring, cyclo[18]carbon: Electronic structure, electronic spectrum, and optical nonlinearity. Carbon 2020; 165: 461–467.

[6] Fedik N, Kulichenko M, Steglenko D, Boldyrev AI. Can aromaticity be a kinetic trap? Example of mechanically interlocked aromatic [2-5]catenanes built from cyclo[18]carbon. Chem Commun 2020; 56(18): 2711−2714.

[7] Charistos ND, Muñoz-Castro A. Induced magnetic field in sp-hybridized carbon rings: Analysis of double aromaticity and antiaromaticity in cyclo[2*N*]carbon

allotropes. Phys Chem Chem Phys 2020; 22(17): 9240–9249.

[8] Li M, Gao Z, Han Y, Zhao Y, Yuan K, Nagase S, Ehara M, Zhao X. Potential molecular semiconductor devices: Cyclo-C_n (n = 10 and 14) with higher stabilities and aromaticities than acknowledged cyclo-C_{18}. Phys Chem Chem Phys 2020; 22(8): 4823–4831.

[9] Dai C, Chen D, Zhu J. Achieving adaptive aromaticity in cyclo[10]carbon by screening cyclo[*n*]carbon (n = 8–24). Chem Asian J 2020; 15(14): 2187–2191.

[10] Liu Z, Lu T, Chen Q. An sp-hybridized all-carboatomic ring, cyclo[18]carbon: Bonding character, electron delocalization, and aromaticity. Carbon 2020; 165: 468–475.

[11] Jiang Y, Wu Y, Deng J, Wang Z. Antiaromaticity-aromaticity transition of cyclo[16]carbon upon metal encapsulation. Phys Chem Chem Phys 2021; 23: 8817–8824.

[12] Fang S, Hu YH. Creating and Seeing the First Pure Carbon Ring. Matter 2019; 1: 1116–1118.

[13] Hussain S, Chen H, Zhang Z, Zheng H. Vibrational spectra and chemical imaging of cyclo[18]carbon by tip enhanced Raman spectroscopy. Chem Commun 2020; 56(15): 2336–2339.

[14] Liu Z, Lu T, Chen Q. Vibrational spectra and molecular vibrational behaviors of all-carboatomic rings, cyclo[18]carbon and its analogues. Chem Asian J 2021; 16: 56–63.

[15] Liu Z, Lu T, Yuan A, Wang X, Chen Q, Yan X. Remarkable Size Effect on Photophysical and Nonlinear Optical Properties of All-Carboatomic Rings, Cyclo[18]carbon and Its Analogues. Chem Asian J 2021; DOI: 10.1002/asia.202100589.

[16] Liu Z, Lu T, Chen Q. Intermolecular interaction characteristics of the all-carboatomic ring, cyclo[18]carbon: Focusing on molecular adsorption and stacking. Carbon 2021; 171: 514–523.

[17] Chen JL, Zhang RQ. Strong Interaction between Cyclo[18]Carbon and Graphene. Adv Theory Simul 2021; 2100022.

[18] Zhang L, Li H, Feng YP, Shen L. Diverse transport behaviors in cyclo[18]carbon-based molecular devices. J Phys Chem Lett 2020; 11(7): 2611–2617.

[19] Jiang Y, Mattioli EJ, Calvaresi M, Wang Z. Theoretical design of an ultrafast supramolecular rotor composed of carbon nano-rings. Chem Commun 2020; 56(79): 11835–11838.

[20] Raeber AE, Mazziotti DA. Non-equilibrium steady state conductivity in cyclo[18]carbon and its boron nitride analogue. Phys Chem Chem Phys 2020; 22(41): 23998–24003.

[21] Hou L, Hu H, Yang G, Ouyang G. Giant Switching Effect and Spintronic Transport Properties in Cyclo[18]carbon-Based Molecular Devices. Phys Status Solidi RRL 2021; 2000582.

[22] Baryshnikov GV, Valiev RR, Nasibullin RT, Sundholm D, Kurten T, Ågren H. Aromaticity of Even-Number Cyclo[*n*]carbons (*n* = 6−100). J Phys Chem A 2020; 124: 10849–10855.

[23] Kozuch S, Nandi A, Solel E. Carbon tunneling in the automerization of cyclo[18]carbon. Chem Eur J 2020; 26(3): 564–753.

[24] Stasyuk AJ, Stasyuk OA, Sol à M, Voityuk AA. Cyclo[18]carbon: The smallest all-carbon electron acceptor. Chem Commun 2020; 56(3): 352−355.

[25] Haley MM. Cyclo[18]carbon, the newest member of the family of carbon allotropes. Chem 2019; 5(10): 2517–2519.

[26] Rahman MZ, Edvinsson T. Rational design and resolution of the mystery of the structure of cyclo[18]carbon. J Mater Chem A 2020; 8(17): 8234–8237.

[27] Pichierri F. Boron-nitrogen analogues of cyclo[18]carbon. Chem Phys Lett 2020; 738: 136860.

[28] Qin B, Zhang Q, Li Y, Yang G, Yu H, Peng F. Mechanistic insights into the electrochemical reduction of CO_2 on cyclo[18]carbon using density functional theory calculations. ChemElectroChem 2020; 7(8): 1838–1842.

[29] Fang S, Hu Y. Cyclo[18]carbon as an ultra-elastic molecular O-ring with unique mechanical properties. Carbon 2021; 171: 96–103.

[30] Liu Z, Lu T, Chen Q. Comment on “Theoretical investigation on bond and spectrum of cyclo[18]carbon (C_{18}) with sp-hybridized”. J Mol Model 2021; 27: 42.

[31] Lu T, Chen Q. Ultrastrong regulation effect of electric field on all-carboatomic ring, cyclo[18]carbon. ChemPhysChem 2021; 22: 386–395.

[32] Xu Y, Wu W. High-efficiency switching effect and negative differential conductance in cyclo[18]carbon–graphene nanoribbon junction. J Appl Phys 2020;

128: 194303.

[33] Hou X, Ren Y, Fu F, Tian X. Doping atom to tune electronic characteristics and adsorption of cyclo[18] carbons: A theoretical study. Comput Theor Chem 2020; 1187: 112922.

[34] Liang Z, He T, An J, Xue H, Tang F, Fan D. Coupling effect and charge redistribution of cyclo[18]carbons and cyclocarbon oxides on NaCl surface. Int J Mod Phys B 2020; 34: 2050138.

[35] Zou W, Tao Y, Kraka E. Systematic description of molecular deformations with Cremer-Pople puckering and deformation coordinates utilizing analytic derivatives: Applied to cycloheptane, cyclooctane, and cyclo[18]carbon. J Chem Phys 2020; 152: 154107.

[36] Domínguez-Gutiérrez FJ, Martínez-Flores C, Krstic PS, Cabrera-Trujillo R, von Toussaint U. Theoretical study of the formation of $C_{18}H$ and $C_{18}H_2$ molecules by low energy irradiation with atomic and molecular hydrogen. Radiat Phys Chem 2021; 179: 109166.

[37] Lo R, Manna D, Hobza P. Cyclo[*n*]carbons Form Strong N → C Dative/Covalent Bonds with Piperidine. J Phys Chem A 2021; 125: 2923−2931.

[38] Brémond É, Pérez-Jiménez AJ, Adamo C, Sancho-García JC. sp-hybridized carbon allotrope molecular structures: An ongoing challenge for density-functional approximations. J Chem Phys 2019; 151: 211104.

[39] Yang Y-F, Cederbaum LS. Endocircular Li Carbon Rings. Angew Chem Int Ed 2021; 60: 16649−16654.

[40] Hoffmann R. Extended Hückel theory-v Cumulenes, polyenes, polyacetylenes and C_n. Tetrahedron 1966; 22(2): 521–538.

[41] Diederich F, Rubin Y, Knobler CB, Whetten RL, Schriver KE, Houk KN, Li Y. All-carbon molecules: Evidence for the generation of cyclo[18]carbon from a stable organic precursor. Science 1989; 245: 1088–1090.

[42] Rubin Y, Knobler CB, Diederich F. Synthesis and crystal structure of a stable hexacobalt complex of cyclo[18]carbon. J Am Chem Soc 1990; 112: 4966–4968.

[43] Rubin Y, Kahr M, Knobler CB, Diederich F, Wilkins CL. The higher oxides of carbon $C_{8n}O_{2n}$ (n = 3–5): Synthesis, characterization, and X-ray crystal structure. Formation of cyclo[*n*]carbon ions C_n^+ (n = 18, 24), C_n^- (n = 18, 24, 30), and higher carbon ions including C_{60}^+ in laser desorption Fourier transform mass spectrometric

experiments. J Am Chem Soc 1991; 113: 495–500.

[44] Tobe Y, Matsumoto H, Naemura K, Achiba Y, Wakabayashi T. Generation of cyclocarbons with 4*n* carbon atoms (C_{12}, C_{16}, and C_{20}) by [2 + 2] cycloreversion of propellane-annelated dehydroannulenes. Angew Chem Int Ed Engl 1996; 35: 1800–1802.

[45] Chai J-D, Head-Gordon M. Long-range corrected hybrid density functionals with damped atom-atom dispersion corrections. Phys Chem Chem Phys 2008; 10(44): 6615–6620.

[46] Weigend F, Ahlrichs R. Balanced basis sets of split valence, triple zeta valence and quadruple zeta valence quality for H to Rn: Design and assessment of accuracy. Phys Chem Chem Phys 2005; 7(18): 3297–3305.

[47] Frisch MJ, Trucks GW, Schlegel HB, Scuseria GE, Robb MA, Cheeseman JR, et al. *Gaussian 16*, revision A.03; Gaussian, Inc.: Wallingford, CT, 2016.

[48] Geuenich D, Hess K, Köhler F, Herges R. Anisotropy of the induced current density (AICD), a general method to quantify and visualize electronic delocalization. Chem Rev 2005; 105(10): 3758–3772, and references therein.

[49] Povray. Persistence of vision raytracer, POV-Ray 3.7: http://www.povray.org/ (accessed on Nov 20, 2019).

[50] Juselius J, Sundholm D, Gauss J. Calculation of current densities using gauge-including atomic orbitals. J Chem Phys 2004; 121(9): 3952–3963.

[51] Breneman CM, Wiberg KB. Determining atom-centered monopoles from molecular electrostatic potentials. The need for high sampling density in formamide conformational analysis. J Comput Chem 1990; 11(3): 361–373.

[52] Lu T, Chen F. Multiwfn: A multifunctional wavefunction analyzer. J Comput Chem 2012; 33(5): 580–592.

[53] Humphrey W, Dalke A, Schulten K. VMD: Visual molecular dynamics. J Mol Graphics 1996; 14(1): 33–38.

[54] Lu T, Chen Q. Interaction Region Indicator: A Simple Real Space Function Clearly Revealing Both Chemical Bonds and Weak Interactions. 2021; 1(5): 231–239.

[55] Schmider HL, Becke AD. Chemical content of the kinetic energy density. J Mol Struct 2000; 527(1–3): 51–61.

[56] Becke AD, Edgecombe KE. A simple measure of electron localization in atomic

and molecular systems. J Chem Phys 1990; 92(9): 5397–5403.

[57] Klod S, Kleinpeter E. Ab initio calculation of the anisotropy effect of multiple bonds and the ring current effect of arenes-application in conformational and configurational analysis. J Chem Soc, Perkin Trans 2001; 22(10): 1893−1898.

[58] Schleyer PvR, Maerker C, Dransfeld A, Jiao H, van Eikema Hommes NJR. Nucleus-independent chemical shifts: a simple and efficient aromaticity probe. J Am Chem Soc 1996; 118(26): 6317−6318.